Fractal stream chemistry and its implications for contaminant transport in catchments

James W. Kirchner*, Xiahong Feng† & Colin Neal#

**Department of Geology and Geophysics, University of California, Berkeley, California 94720-4767, USA*
† Department of Earth Sciences, Dartmouth College, Hanover, New Hampshire 03755, USA
 # Institute of Hydrology, McLean Building, Wallingford, Oxon OX10 8BB, UK

The time it takes for rainfall to travel through a catchment and reach the stream is a fundamental hydraulic parameter that controls the retention of soluble contaminants and thus the downstream consequences of pollution episodes[1,2]. Catchments with short flushing times will deliver brief, intense contaminant pulses to downstream waters, whereas catchments with longer flushing times will deliver less intense but more sustained contaminant fluxes. Here we analyse detailed time series of chloride, a natural tracer, in both rainfall and runoff from headwater catchments at Plynlimon, Wales. We show that, although the chloride concentrations in rainfall have a white noise spectrum, the chloride concentrations in streamflow exhibit fractal 1/*f* scaling over three orders of magnitude. The fractal fluctuations in tracer concentrations indicate that these catchments do not have characteristic flushing times. Instead, their travel times follow an approximate power-law distribution implying that they will retain a long chemical memory of past inputs. Contaminants will initially be flushed rapidly, but then low-level contamination will be delivered to streams for a surprisingly long time.

A catchment is characterized by a distribution of travel times, reflecting the diverse flow paths that rainfall can take to the stream. Quantifying this travel time distribution is essential for predicting the transport of water and solutes, including soluble contaminants. Catchments are spatially complex and subsurface flow is invisible, so one can only infer the movement and mixing of waters from the isotopic and chemical tracers that they carry. Chloride is an effective chemical tracer[3], because it is nonreactive under typical catchment conditions. Our three small (1.0–3.5 km^2) study catchments[4] are close to the Welsh coastline, and sea-salt chloride inputs fluctuate greatly from one storm to the next. By comparing the chloride signatures of rainfall and runoff through time, we can measure how long the catchments retain a chemical memory of the rain that has fallen in them[5,6]. We measured chloride in rainfall and streamflow at two different temporal resolutions: weekly for 14 years (780 data points), and daily for over three years (1,140 data points). In both data sets, rainfall concentrations are volume-weighted averages over the preceding day or week, whereas streamflow concentrations are instantaneous values at the time of sampling.

The daily hydrograph (Fig. 1a) shows that storm rainfall inputs are usually matched by prompt (and roughly equal) changes in streamflow. By contrast, streamflow chloride response to storm inputs is strongly damped (Fig. 1b), indicating that peak flows consist mostly of pre-storm water released from the catchment, rather than rainfall flowing directly into the stream[6] (storm response at Plynlimon, as at many forested catchments, is dominated by groundwater flow and interflow, with return flow occurring at the bases of some slopes[7–9]). This rapid release of 'old' water[10,11] implies that our catchments transmit hydrologic signals from rainfall to runoff much more rapidly and distinctly than chemical signals. This decoupling of timescales occurs because fluctuations in hydraulic head (which drives water to the stream) can propagate much faster than the water itself[12].

The timescales of catchment hydrologic and chemical response can be clarified using spectral methods[13,14], which decompose the rainfall and streamflow signals into their component wavelengths. By comparing the spectral power of the input (rainfall) and output (streamflow) at each wavelength, we can determine how strongly the catchment attenuates hydrologic and chemical signals on each timescale. The spectra of water fluxes in rainfall and streamflow lie nearly on top of one another (Fig. 2a), indicating that all three catchments transmit hydrologic signals with little damping, on all but the shortest timescales.

By contrast, the spectra of the streamflow chloride concentrations (Fig. 2b) show strong attenuation on all wavelengths shorter than 5–10 years, with progressively greater attenuation at shorter wavelengths. Except for a strong annual peak (and its subharmonics) reflecting seasonal fluctuations, the rainfall chloride spectrum scales roughly as white noise. The streamflow chloride spectra, by contrast, show fractal power-law scaling that resembles 1/*f* noise (Fig.

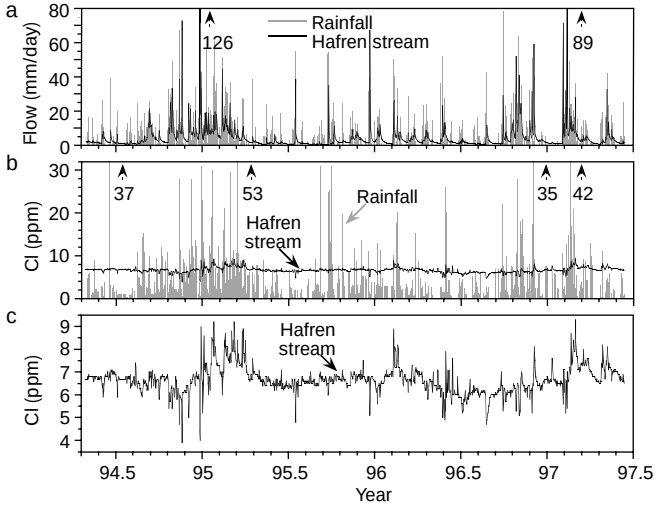

Figure 1 Time series of daily water fluxes and chloride concentrations. **a**, **b**, At the Hafren catchment, Plynlimon, Wales, hydrologic response to rainfall inputs (**a**) is prompt, with little attenuation, but chemical response (**b**) is strongly damped. Peaks beyond plot axes are labelled individually. **c**, Enlarged view of the stream chloride time series shows that it exhibits both short-term transience and long-term persistence. For details of measurement methods see ref. 3.

2b), with spectral power inversely proportional to frequency; this indicates that catchments can act as fractal filters, converting white noise inputs into $1/f$ noise outputs. The fractal scaling in the streamflow chloride spectra is consistent between the daily and weekly data sets, consistent among five sampling sites in our three study catchments (see Supplementary Information), and consistent across timescales spanning three orders of magnitude—a wider range of scales than is usually used to characterize fractal behaviour[15].

We have also tested the generality of these results using long (8–30 year) time series of weekly chloride measurements in nine Scandinavian and North American streams; eight of the nine exhibit fractal power-law scaling, between $1/f^{0.7}$ and $1/f^{1.2}$, over 1.5–2.5 orders of magnitude. Whereas the Plynlimon catchments are underlain by deeply fractured shale, the Scandinavian and North American catchments mostly lie on glaciated granitic and metamorphic rocks and thus are much less permeable at depth. The prevalence of fractal scaling means that it does not require unusual catchment characteristics.

The damping of tracer fluctuations from rainfall to streamflow can be used to infer a catchment's travel time distribution[16,17]. Each day's rainfall influences stream chemistry in future days, by an amount that is determined by the travel time distribution. Equivalently, the present concentration in the stream reflects the rainfall concentrations throughout the past, weighted by their fractional contribution to the present runoff. Mathematically this means that the stream concentration $c_S(t)$ at any time t is the convolution of the travel time distribution $h(\tau)$ and the rainfall concentration $c_R(t-\tau)$ throughout the past, where τ is the lag time between rainfall and runoff:

$$c_S(t) = \int_0^\infty h(\tau)c_R(t-\tau)\mathrm{d}\tau \quad (1)$$

Because the flow rate varies through time, equation (1) is strictly valid when t and τ are expressed in terms of the cumulative flow through the catchment, rather than calendar time[18,19], but the mathematics are the same in either case[19]. We performed the following analysis both ways and obtained functionally equivalent results, so for simplicity we use the time-based formalism below.

From equation (1) one can see that if a catchment's travel time distribution is broad compared to the wavelength of a chemical signal in the rainfall, signals travelling by different flow paths will tend to average each other out when they reach the stream. Thus the average concentration will be maintained, but fluctuations will be

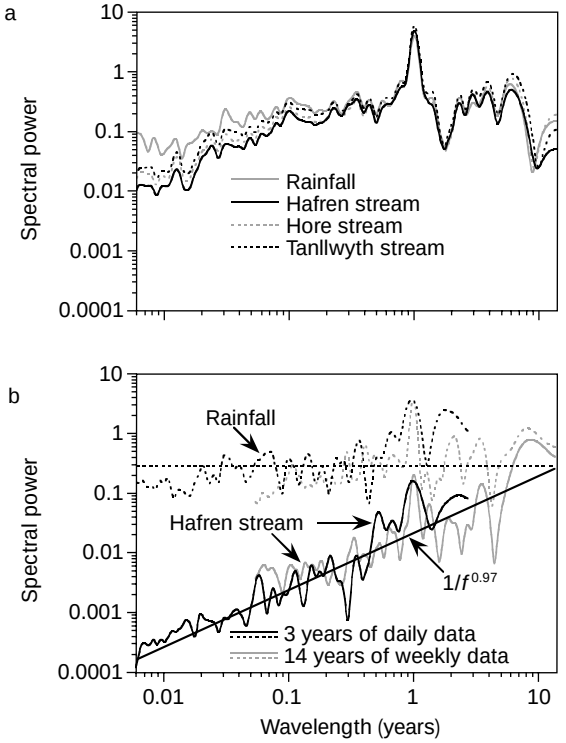

Fig. 2 Power spectra of water fluxes and chloride concentrations. Water flux (rainfall and streamflow) spectra (**a**) indicate little damping, except at the shortest timescales, whereas chloride concentration spectra (**b**) show strong attenuation, except at the longest timescales. Chloride spectra of rainfall (dotted lines) resemble white noise; those of streamflow (solid lines) resemble $1/f$ noise, with spectral power increasing proportionally to wavelength across the entire range of scales. For ease of interpretation, spectra are shown as functions of wavelength (reciprocal of frequency) rather than frequency. **a,** Data are daily for 14 years**; b,** data are daily for 3 years, or weekly for 14 years (see figure). Hafren, Hore and Tanllwyth are adjacent catchments at Plynlimon, Wales.

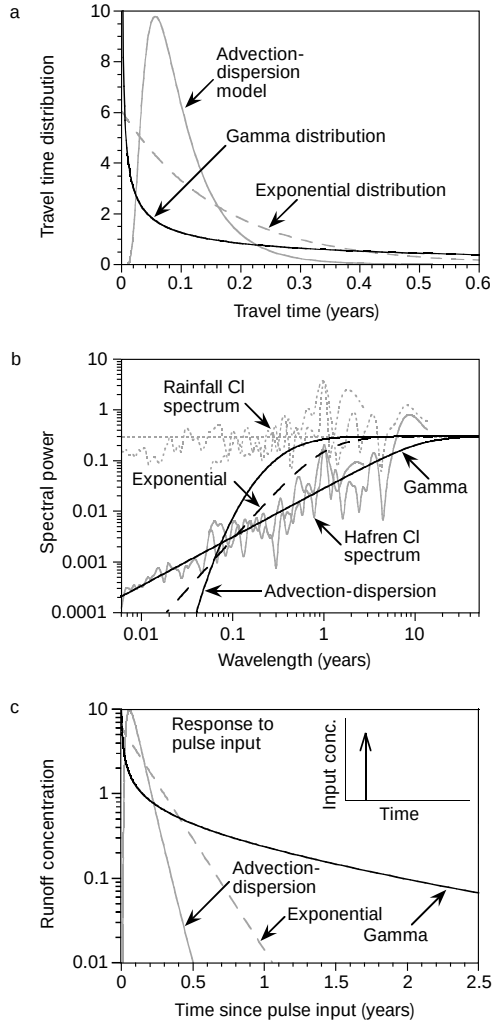

Figure 3 Travel time distributions and their implications for contaminant transport. **a**, Power-law (gamma) distribution compared to two conventional models for catchment travel times (advection–dispersion and exponential). **b**, Power spectra of the three distributions, superimposed on the rainfall and Hafren chloride concentration spectra. Modelled power spectra assume that the rainfall concentration spectrum is white noise (straight dotted line). **c**, Response of streamflow concentrations to a delta-function pulse input of contaminants. Because the gamma distribution has a much longer tail than the conventional models, it sustains substantial contaminant concentrations for much longer time spans. The logarithmic concentration scale emphasizes the persistence of low-level contamination. Inset depicts delta-function contaminant input.

attenuated. The shorter the wavelength of the chemical fluctuation in rainfall compared to the catchment's travel time distribution, the stronger this attenuation by averaging becomes. Conversely, chemical variations on timescales that are long compared to the travel time distribution will be transmitted through the catchment without significant attenuation. By the convolution theorem, equation (1) implies that[20]:

$$C_S(f) = H(f)C_R(f) \quad \text{and} \quad |C_S(f)|^2 = |H(f)|^2|C_R(f)|^2 \quad (2)$$

Here f is frequency; $C_S(f)$, $H(f)$ and $C_R(f)$ are the Fourier transforms of $c_S(t)$, $h(\tau)$ and $c_R(t-\tau)$; and $|C_S(f)|^2$, $|H(f)|^2$ and $|C_R(f)|^2$ are their power spectra. In our case, because the rainfall concentration spectrum is nearly white noise ($|C_R(f)|^2$ is approximately constant), the spectrum of the travel time distribution is roughly proportional to the runoff concentration spectrum ($|H(f)|^2 \propto |C_S(f)|^2$). From equation (2) it is clear that the power-law scaling observed in Fig. 2b can arise only if the travel time distribution is an approximate power function of the form $h(\tau) \propto \tau^{-m}$ with $m \approx 0.5$. It is equally clear that this approximation must break down for large τ, because otherwise the average travel time would become infinite. (No such difficulty occurs for small τ, since τ^{-m} ($0 < m < 1$) is integrable, though unbounded, at $\tau = 0$.) An approximate power function that is integrable at large τ is the gamma distribution (Fig. 3a):

$$h(\tau) = \frac{\tau^{\alpha-1}}{\beta^{\alpha}\Gamma(\alpha)} e^{-\tau/\beta} \quad (3)$$

Here β is a scale parameter and $\alpha = 1 - m \approx 0.5$ is a shape parameter. With a fitted value of $\alpha = 0.48 \pm 0.01$, the gamma distribution's power spectrum[21]

$$|H(f)|^2 = (1 + 4\pi^2 f^2 \beta^2)^{-\alpha} \quad (4)$$

agrees well with the observed power spectrum (Fig. 3b), scaling as $f^{-2\alpha} \approx f^{-0.97}$ for $2\pi f\beta \gg 1$. The gamma distribution has previously been used to model catchment travel times[22], but with $\alpha \geqslant 1$ rather than $\alpha \approx 0.5$, for which it has a completely different shape.

Figure 3 contrasts the gamma distribution with two distributions that are often used to model travel times in catchments. If catchments are modelled as well-mixed reservoirs, their travel times follow an exponential distribution[16,18,22], which is equivalent to equation (3) with $\alpha = 1$. Thus a well-mixed reservoir also exhibits power-law scaling, but with a non-fractal slope of 2, rather than the observed fractal slope of ~1 (Fig. 3b). Alternatively, if solutes are assumed to reach the stream by transport and dispersion along a single flow path, their travel times are described by the advection–dispersion equation[23–25], whose power spectrum[16] shows no power-law scaling (Fig. 3b). Both of these alternative models strongly attenuate fluctuations below some characteristic timescale; thus they will either greatly overestimate the attenuation of short-term fluctuations, or greatly underestimate the timescales required for output concentrations to track inputs (and thus the flushing time for the catchment). The stream concentration time series (Fig. 1c) and spectrum (Fig. 2b) indicate that the catchment exhibits both short-term responsiveness to input fluctuations, and long-term memory of past inputs. Only the approximate power-law distribution (equation (3)) has both of these characteristics.

Our finding that tracer fluctuations in streams are fractals, and thus that catchment travel time distributions are approximate power functions, has important implications for contaminant retention by catchments. Conventional methods for predicting cleanup timescales assume that solute travel times follow either an exponential or advection–dispersion distribution[26]. Compared to those distributions, equation (3) is much steeper at very short lags, but converges toward zero very slowly for long lag times (Fig. 3a). This implies that after pollution episodes, contaminant concentrations will fall rapidly at first, but then decline much more gradually (Fig. 3c). Expectations based on the initial rapid drop will be thwarted by the persistence of contaminant concentrations over the long term. This persistence may be further amplified by adsorption/desorption reactions between contaminants and mineral surfaces ("retardation"), which do not affect our chloride tracer.

Soil pores and bedrock fractures exhibit fractal scaling[27,28], which may be related to the power-law distribution of travel times and the fractal structure of stream chemistry fluctuations. However, catchment travel time distributions are also shaped by many other factors: the spatial distribution of rainfall, the length, tortuosity, and velocity of the flowpaths connecting the stream to each point on the surface, dispersion along and between flowpaths, and diffusive exchange between mobile water in macropores and immobile water in the matrix between them[24]. The travel time distribution (equation (3)) and power spectra (Fig. 2) presented here provide important observational constraints on the physical processes controlling water flow, storage, and mixing at catchment scale. Understanding these processes, and their implications for water quality, is a critical challenge in the environmental sciences[29]. □

Methods

Power spectra

Because rainfall chloride concentrations are undefined on dates without rain, we calculated power spectra using the Lomb–Scargle Fourier transform[14], which has the same statistical properties as the conventional Fast Fourier Transform, but does not require evenly spaced data. We omitted Scargle's prefactor of $(N_o/2)^{1/2}$ in order to make spectral power comparable between the daily and weekly data sets, which have different numbers of points.

Travel time distributions

The power spectra of all three travel time distributions were fitted to the stream chloride spectra (Fig. 3b) by least squares. The gamma distribution is equation (3), with parameter values of $\alpha = 0.48 \pm 0.01$ and $\beta = 1.9 \pm 0.1$ years (corresponding to an average travel time of $\alpha\beta = 0.9$ years). The power-law slope of its spectrum is controlled by α, and its left-to-right location is controlled by β. The exponential distribution is equation (3) with α fixed at 1 and a fitted mean travel time of $\alpha\beta = 0.16 \pm 0.01$ years. The advection–dispersion model is equation (11) of Kreft and Zuber[23], with an assumed Peclet number of 5 and a fitted mean travel time of 0.10 ± 0.01 years; other realistic Peclet numbers yield equally poor fits to the data.

Received 24 May; accepted 1 November 1999.

1. Langmuir, D. *Aqueous Environmental Geochemistry* (Prentice-Hall, Upper Saddle River, New Jersey, 1997).
2. Schnoor, J. L. *Environmental Modeling: Fate and Transport of Pollutants in Water, Air, and Soil* (Wiley, New York, 1996).
3. Neal, C. & Rosier, P. T. W. Chemical studies of chloride and stable oxygen isotopes in 2 conifer afforested and moorland sites in the British uplands. *J. Hydrol.* **115,** 269–283 (1990).
4. Neal, C. *et al.* The hydrochemistry of the River Severn, Plynlimon. *Hydrol. Earth Syst. Sci.* **1,** 583–617 (1997).
5. Robson, A., Neal, C., Hill, S. & Smith, C. J. Linking variations in short-term and medium-term stream chemistry to rainfall inputs – some observations at Plynlimon, mid-Wales. *J. Hydrol.* **144,** 291–310 (1993).
6. Neal, C. *et al.* Chloride in precipitation and streamwater for the upland catchment of the River Severn, mid-Wales: some consequences for hydrochemical models. *Hydrol. Process.* **2,** 155–165 (1988).
7. Kirkby, C., Newson, M. D. & Gilman, K. *Plynlimon research; the first two decades* (Institute of Hydrology Report 109, Institute of Hydrology, Wallingford, UK, 1991).
8. Neal, C., Hill, T. & Reynolds, B. Acid neutralisation capacity measurements in surface and groundwaters in the upper River Severn, Plynlimon: from hydrograph splitting to water flow pathways. *Hydrol. Earth Syst. Sci.* **1,** 687–696 (1997).
9. Neal, C. *et al.* The occurrence of groundwater in the lower Palaeozoic rocks of upland Wales. *Hydrol. Earth Syst. Sci.* **1,** 3–18 (1997).
10. Buttle, J. M. Isotope hydrograph separations and rapid delivery of pre-event water from drainage basins. *Prog. Phys. Geog.* **18,** 16–41 (1994).
11. Sklash, M. G., Beven, K. J., Gilman, K. & Darling, W. G. Isotope studies of pipeflow at Plynlimon, Wales, UK. *Hydrol. Process.* **10,** 921–944 (1996).
12. Beven, K. On subsurface stormflow: predictions with simple kinematic theory for saturated and unsaturated flows. *Wat. Resour. Res.* **18,** 1627–1633 (1982).
13. Bracewell, R. N. *The Fourier Transform and its Applications* 3rd edn (McGraw-Hill, Boston, 2000).
14. Scargle, J. D. Studies in astronomical time series analysis. II. Statistical aspects of spectral analysis of unevenly spaced data. *Astrophys. J.* **263,** 835–853 (1982).
15. Avnir, D., Biham, O., Lidar, D. & Malcai, O. Is the geometry of nature fractal? *Science* **279,** 39–40 (1998).
16. Duffy, C. J. & Gelhar, L. W. A frequency domain approach to water quality modeling in groundwater: theory. *Wat. Resour. Res.* **21,** 1175–1184 (1985).
17. Duffy, C. J. & Gelhar, L. W. A frequency domain analysis of groundwater quality fluctuations: interpretation of field data. *Wat. Resour. Res.* **22,** 1115–1128 (1986).

18. Rodhe, A., Nyberg, L. & Bishop, K. Transit times for water in a small till catchment from a step shift in the oxygen-18 content of the water input. *Wat. Resour. Res.* **32,** 3497–3511 (1996).
19. Niemi, A. J. Residence time distributions of variable flow processes. *Int. J. Appl. Radiat. Isotopes* **28,** 855–860 (1977).
20. Gelhar, L. W. *Stochastic Subsurface Hydrology* (Prentice-Hall, Englewood Cliffs, NJ, 1993).
21. Bain, L. in *Encyclopedia of Statistical Sciences* (eds. Kotz, S. & Johnson, N. L.) 292–298 (Wiley, New York, 1983).
22. Turner, J. V. & Barnes, C. J. in *Isotope Tracers in Catchment Hydrology* (eds Kendall, C. & McDonnell, J. J.) 723–760 (Elsevier, Amsterdam, 1998).
23. Kreft, A. & Zuber, A. On the physical meaning of the dispersion equation and its solutions for different initial and boundary conditions. *Chem. Eng. Sci.* **33,** 1471–1480 (1978).
24. Sposito, G., White, R. E., Darrah, P. R. & Jury, W. A. A transfer function model of solute transport through soil 3. The convection-dispersion equation. *Wat. Resour. Res.* **22,** 255–262 (1986).
25. Stewart, M. K. & McDonnell, J. J. Modeling base flow soil water residence times from deuterium concentrations. *Wat. Resour. Res.* **26,** 3005–3019 (1991).
26. Kavanaugh, M. C. *et al. Alternatives for Ground Water Cleanup* (National Academy Press, Washington, DC, 1994).
27. Turcotte, D. L. *Fractals and Chaos in Geology and Geophysics* (Cambridge University Press, 1992).
28. Korvin, G. *Fractal Models in the Earth Sciences* (Elsevier Science, Amsterdam, 1992).
29. Neal, C. A view of water quality from the Plynlimon watershed. *Hydrol. Earth Syst. Sci.* **1,** 743–754 (1997).

Supplementary information is available on *Nature*'s World-Wide Web site (http://www.nature.com) or as paper copy from the London editorial office of Nature.

Acknowledgements

Our collaboration was supported by a National Science Foundation grant to J.W.K. Sample collection and analysis were supported by the Natural Environment Research Council, the Environment Agency of England and Wales, and the Forestry Commission. We thank the Plynlimon field staff for sample collection, M. Neal for sample analysis, C. Stark for comments on the manuscript, and D. Brillinger for helpful advice.

Correspondence and requests for materials should be addressed to J.W.K. (e-mail: kirchner@seismo.berkeley.edu).

Rapid diffusive infiltration of sodium into partially molten peridotite

Craig C. Lundstrom

Department of Geological Sciences, Brown University, Providence, Rhode Island 02912, USA
Present address: Department of Geology, University of Illinois, Urbana, Illinois 61801, USA.

Recent seismological, geochemical and experimental observations suggest that, as mantle peridotite melts, the resulting basaltic liquid forms an interconnected network, culminating in the rapid ascent of the basalt relative to the surrounding solid matrix[1–3]. Mantle melting is therefore a polybaric process, with melts produced over a range of pressures having differing chemical characteristics[4–6]. Modelling and peridotite-melting experiments designed to simulate polybaric mantle melting generally assume that there is no interaction between melts generated at greater pressures and the overlying solid mantle at lower pressures[5,7]. Beneath mid-ocean ridges, melts derived from greater depth are probably channelized during ascent, so preventing direct re-equilibration with shallow peridotite[8], as required by geochemical observations[6,9]. I show here, however, that sodium in ascending melts will quickly diffuse into the melt formed within nearby peridotite at lower pressures. This process fundamentally changes the manner by which the peridotite melts, and can account for both the creation of silica-rich glass inclusions in mantle xenoliths and the anomalous melting modes recorded by abyssal peridotites. Increased melting of lithosphere and upwelling asthenosphere could result from this process without the need to invoke higher mantle temperatures.

On the basis of experimental results, early formed high-pressure melts derived from the base of a melting column will be lower in SiO_2 and higher in Na_2O than larger-degree melts in equilibrium with mantle peridotite at shallow depths[10,11]. To simulate the interaction between a melt originally generated at greater pressures and peridotite at lower pressure, a two-step experiment was performed in a piston cylinder apparatus at 1,300 °C and 0.9 GPa using salt–Pyrex assemblies (10% friction correction). The initial synthesis runs (30 hours) produced (1) a peridotite coexisting with ~10% tholeiitic glass (starting material was spinel therzolite KLB-1[12]) and (2) a basanitic glass coexisting with ~10% olivine (starting material was EL-10 from the Canary Islands, collected by K. Hoernle), both enclosed in graphite inner capsules sealed inside Pt-lined Mo outer capsules. After synthesis, a portion of each of these materials was removed for analysis. The capsules were then each polished flat on one end and juxtaposed in the piston cylinder for 10 minutes under the same conditions of temperature and pressure. The peridotite–basanite interface after reaction remained well defined and fixed in its original location; however, peridotite close to the interface contained more melt than did peridotite far from the interface (Fig. 1).

Compositions of melt pools within the peridotite vary as a

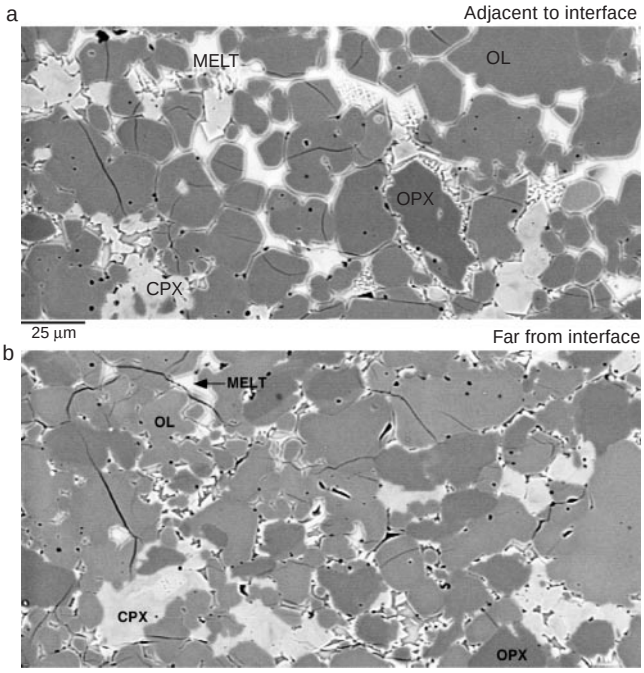

Figure 1 Back-scattered electron (BSE) images of peridotite. **a,** Closest to the basanite–peridotite interface; **b,** farthest from the interface. Note the clear difference in melt and mineral modes between the two regions of the experiment. Representative minerals are labelled (orthopyroxene (OPX), dark grey; olivine (OL), medium grey; clinopyroxene (CPX) and MELT, both light grey) with lighter jagged edges on pyroxenes and lighter rims on olivine resulting from quench crystallization. In order to quantify phase proportions in the experiment (Fig. 3), four non-overlapping, digital BSE images (250 μm^2) and Mg X-ray maps were simultaneously collected throughout the peridotite portion of the sample in each of four rows that varied as a function of distance from the original peridotite–basanite interface (see Fig. 2 for locations of rows). Each image was processed using NIH Image software with mineral modes calculated by summing areas of particular grey scale. With the aid of Mg X-ray maps, melt, orthopyroxene and clinopyroxene were distinguished from olivine and the mode of each was counted after selectively darkening phases using imaging software. For each row, an average mode and 1 standard deviation (s.d.) were calculated from the four images. Quench crystals could be readily distinguished from the primary minerals; the melt mode reflects the area covered by both melt and quench crystals. Cracks and surface imperfections (black) are not included in the modal determination.